NASA Technical Memorandum 107184

Single Transducer Ultrasonic Imaging Method That Eliminates the Effect of Plate Thickness Variation in the Image

Don J. Roth
Lewis Research Center
Cleveland, Ohio

July 1996

National Aeronautics and
Space Administration

SINGLE TRANSDUCER ULTRASONIC IMAGING METHOD THAT ELIMINATES THE EFFECT OF PLATE THICKNESS VARIATION IN THE IMAGE

Don J. Roth

National Aeronautics and Space Adminstration

Lewis Research Center

Cleveland, Ohio 44135

ABSTRACT

This article describes a single transducer ultrasonic imaging method based on ultrasonic velocity measurement that eliminates the effect of plate thickness variation in the image, i.e. the method is thickness-independent. The method, currently being commercialized under a cooperative agreement between NASA Lewis Research Center and Sonix, Inc., thus isolates ultrasonic variations due to material microstructure. Its use can result in significant cost savings because the ultrasonic image can be interpreted correctly without the need for precision thickness machining during nondestructive evaluation stages of material development. Images obtained using the thickness-independent methodology are compared with apparent velocity maps and c-scan echo peak amplitude images for monolithic ceramic (silicon nitride), metal matrix composite and polymer matrix composite materials having thickness and microstructural variations. It was found that the thickness-independent ultrasonic images reveal and quantify correctly areas of global microstructural (pore and fiber volume fraction) variation due to the elimination of thickness effects.

ACKNOWLEDGMENTS

The author wishes to thank Dr. James K. Sutter from NASA Lewis Research Center, Dr. Kamal Amin of 3M Co., and Mr. James R. Bodis of Cleveland State University for their help in providing samples and general assistance during this investigation.

INTRODUCTION

Ultrasonic c-scan imaging is an effective nondestructive evaluation (NDE) technique used for materials analysis and quality control in the aerospace, electronics, and other industries (Ref. 1). C-scan imaging in its most conventional implementation is used to map variations in ultrasonic echo peak amplitude that occur when scanning across a material part (Ref. 1). In the *pulse-echo* c-scan configuration, echoes that are sometimes monitored or "gated" include those reflecting off the sample front and back surfaces (Ref. 1). For currently available commercial scan systems, the amplitude variations are generally scaled to values between zero and 255 [8-bit dynamic range] and displayed on video in terms of gray or color scale. In this manner, gray scale variations in the image are associated with amplitude, or attenuation, variations. An additional implementation of c-scan imaging involves mapping variations in the time of occurrence of an ultrasonic echo peak with respect to a reference time. These "time-of-flight" variations are scaled and displayed in a similar fashion to echo peak amplitude. Both amplitude and time-of-flight variations of a *back surface* echo are many times related to variations in a volumetric microstructural property such as density which can affect physical material properties such as stiffness and thermal conductivity. However, a weakness of conventional ultrasonic c-scan imaging regarding both peak amplitude and time-of-flight modes is that gray scale variations in images for *back surface* reflections indicate part thickness variations as well as microstructural variations unless the part is uniformly thick.

BACKGROUND

By their very nature, both peak amplitude and time-of-flight measurements are directly dependent on thickness. Peak amplitude (A) is affected by thickness according to the expression for pulse-echo attenuation where (Ref. 1):

$$A = A_o \exp(-\alpha[2d]) \tag{1}$$

where A_o is an initial reference amplitude, α is the material attenuation coefficient, and d is the thickness of the part. In practical application, the severity of the effect of thickness variation on peak amplitude depends on the frequency of ultrasound used because the ultrasonic attenuation coefficient normally increases with increasing frequency. Generally it is desirable to use the highest frequency of ultrasound possible to maximize resolution of non-uniformity. As an example of the effect of thickness variations on peak amplitude, Fig. 1 shows the effect of thickness on back wall ultrasonic signals obtained from PMR-15 polyimide samples for pulse-echo experiments

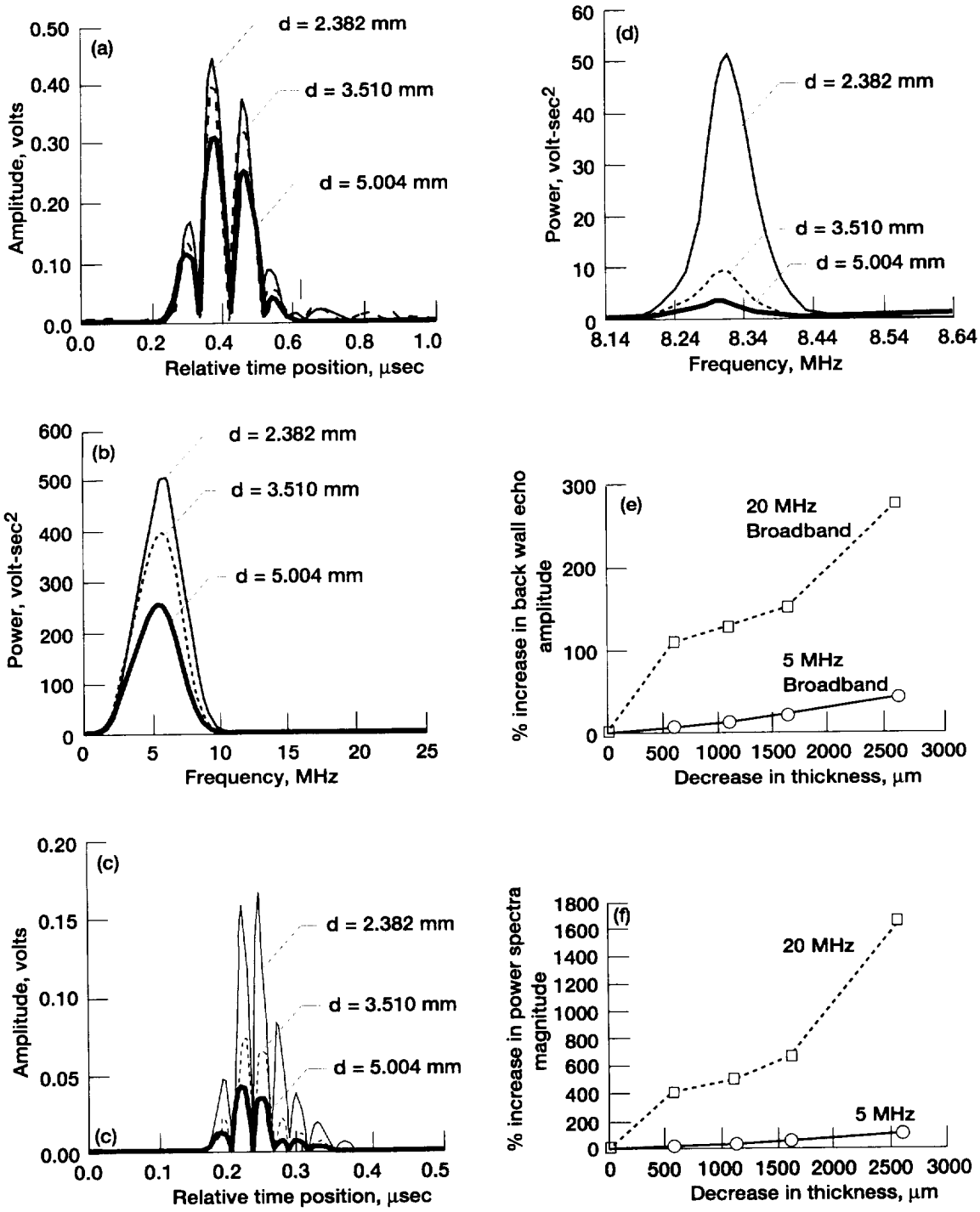

Figure 1.—Effect of thickness on ultrasonic echo peak amplitude for PMR-15 polymide sample. d = thickness. (a) Rectified back wall echo for three thicknesses using 5 MHz broadband transducer. (b) Fourier power spectra of back wall echo for three thicknesses using 5 MHz broadband transducer. (c) Rectified back wall echo for three thicknesses using 20 MHz broadband transducer. (d) Fourier power spectra of back wall echo for three thicknesses using 20 MHz broadband transducer. (e) Percent increase in back wall echo peak amplitude versus decrease in thickness. (f) Percent increase in power spectra magnitude versus decrease in thickness.

conducted at NASA Lewis Research Center. Thickness of the samples ranged from ~2.3 to 5 mm. The experiments were conducted using both 5 and 20 MHz broadband transducers. Results are shown for both the time-domain broadband back wall pulse (Figs. 1(a), (c) and (e)) and the frequency-domain power spectra of the pulse (Figs. 1(b), (d) and (f)). Figure 1 illustrates that the back wall echo amplitude increases with decreasing thickness at both frequencies, but much more significantly so at 20 MHz than at 5 MHz due to the considerably higher attenuation coefficient at 20 MHz for PMR-15 material ($\alpha_{PMR\text{-}15}$ at 20 MHz = 2.761 ± 0.2 Neper/cm and $\alpha_{PMR\text{-}15}$ at 5 MHz = 1.184 ± 0.1 Neper/cm as obtained from experiments at Lewis). These results indicate that results of peak amplitude c-scans including the effect of thickness variations will be highly frequency-dependent.

The situation is more straight forward for interpreting the effect of thickness variations on time-of-flight of ultrasonic pulses off the sample back wall. Back wall pulse-echo time-of-flight (2τ) is affected by thickness variation according to:

$$2\tau = \frac{(2d)}{V} \tag{2}$$

where V is the velocity of ultrasound in the material. No frequency dependence exists as does for attenuation (disregarding dispersion effects of frequency on material velocity (V)). Thickness effects on time-of-flight can also be interpreted by rearranging Eq. (2) to calculate velocity according to:

$$V = \frac{(2d)}{(2\tau)} \tag{3}$$

such that velocity is inversely proportional to time-of-flight. For velocity mapping from scan results, only one thickness value can be used practically in the velocity map calculation (Eq. (3)). This value is usually an average value obtained from several measurements at different sample locations. For scan locations where actual thickness is less than the value chosen for the calculation, time-of-flight will be less, and *apparent* velocity will be greater, than that if the scan location had the chosen value of thickness. The situation is opposite for scan locations where actual thickness is greater than the value chosen for the calculation. Hence, velocity and time-of-flight maps will be affected similarly by thickness variations, and velocity maps are used in this investigation to indicate time-of-flight variations.

Since the attenuation coefficient (α) and velocity (V) in a material will not be constant if microstructural variations are present, Eqs. (1) to (3) indicate that maps of peak amplitude, time-of-flight, and velocity will show a combination of microstructural and thickness variations.

PRIOR ART

Several attempts to account for thickness variation effects in ultrasonic images were noted in the literature (Refs. 2 and 3). Reference 2 used a two-transducer method whereby the transducers were used in both pulse-echo and through-transmission mode to monitor thickness via time-of-flight information and track echo peak amplitude. Knowing the thickness at each scan location, the material attenuation coefficient, and the assumption that the attenuation coefficient is constant throughout the part, a c-scan image can be produced free of thickness effects. Ref. 3 used an ultrasonic velocity imaging method combined with error analysis methodology to define the percent velocity variation due to each of thickness and microstructural variation in a velocity image. This allowed one to conclude whether the percent variation seen in the velocity image was due to thickness variation, microstructural variation, or a combination of the two. However, this methodology allowed only a global generalization and the image itself could not be changed to eliminate thickness effects. Several references showed single point (non-imaging) ultrasonic measurement methodology that accounted for thickness variation effects (Refs. 4 and 6). The method of Ref. 4 simultaneously determined ultrasonic velocity, plate thickness and wedge angle and conceivably could be extended to imaging. However, it is most applicable to samples having "regular" thickness variation such as for a wedge shape. References 5 and 6 described a single point ultrasonic velocity measurement method using a reflector plate located behind the sample that does not require prior knowledge of sample thickness and lends itself to multiple measurements within a sample of nonuniform thickness.

SCOPE OF INVESTIGATION

In this investigation, the methods of Refs. 5 and 6 are engineered to perform automated imaging so that the resultant velocity image is free of thickness variation effects, i.e. is thickness-independent. Results are shown as obtained from a lab-based prototype system and a commercial c-scan system in which the method of this article was implemented under a NASA - industry (Sonix, Inc., 8700 Morrissette Drive, Springfield, VA 22152) cooperative agreement (Ref. 7). Scans are performed on silicon nitride ceramic, metal matrix composite, and polymer matrix composite materials containing microstructural and thickness variations. Thickness-independent ultrasonic images for these materials are compared to c-scan peak amplitude images and conventional (apparent) velocity images obtained using Eq. (3).

THICKNESS-INDEPENDENT VELOCITY IMAGING METHODOLOGY

A pulse-echo ultrasonic velocity measurement is generally made with a transducer either contacting the sample (contact mode) or separated by a liquid coupling path (immersion mode). Figure 2 shows a schematic of immersion pulse-echo testing and resulting waveforms with a reflector plate positioned underneath, and separated from, the sample. Conventional velocity (V) values as obtained from Eq. (3) are calculated using the time delay (2τ) between the first front surface and first back surface echo, or between 2 successive back surface echoes, according to Eq. (3).

The pulse-echo immersion method described by Refs. 5 and 6 for measuring velocity in a material sample uses echoes off of the reflector plate as well as front and/or back surface echoes. The following steps show how velocity (V) in a sample of thickness (d) is determined without needing prior knowledge of thickness. Notation consistent with that of Ref. 6 is used. With the sample present between the transducer and the reflector plate (Fig. 2), the pulse that travels from the transducer through the sample to the reflector plate and back to the transducer is labeled M' and will be observed at time t' where:

$$t' = \left(2t_1 + 2\tau + 2t_2\right) \tag{4}$$

where $2t_1$, 2τ, and $2t_2$ are the pulse-echo time delays of the ultrasonic pulse from the transducer face to the sample front surface, from the sample front surface to the sample back surface, and from the sample back surface to the reflector plate front surface, respectively (Fig. 2(b)). With the sample removed, the pulse that travels from the transducer to the reflector plate and back to the transducer is labeled M'' and will be observed at time t'' where:

$$t'' = \left(2t_1 + 2\frac{d}{c} + 2t_2\right) \tag{5}$$

where c is the temperature-dependent velocity of sound in water. (In this case with the sample removed, $2t_2$ is the pulse-echo time delay of the ultrasonic pulse from a point equivalent to the sample back surface to the reflector plate front surface and is equal to $2t_2$ noted originally.) Subtracting Eq. (4) from Eq. (5) gives:

$$t'' - t' = \Delta t = 2\frac{d}{c} - 2\tau \tag{6}$$

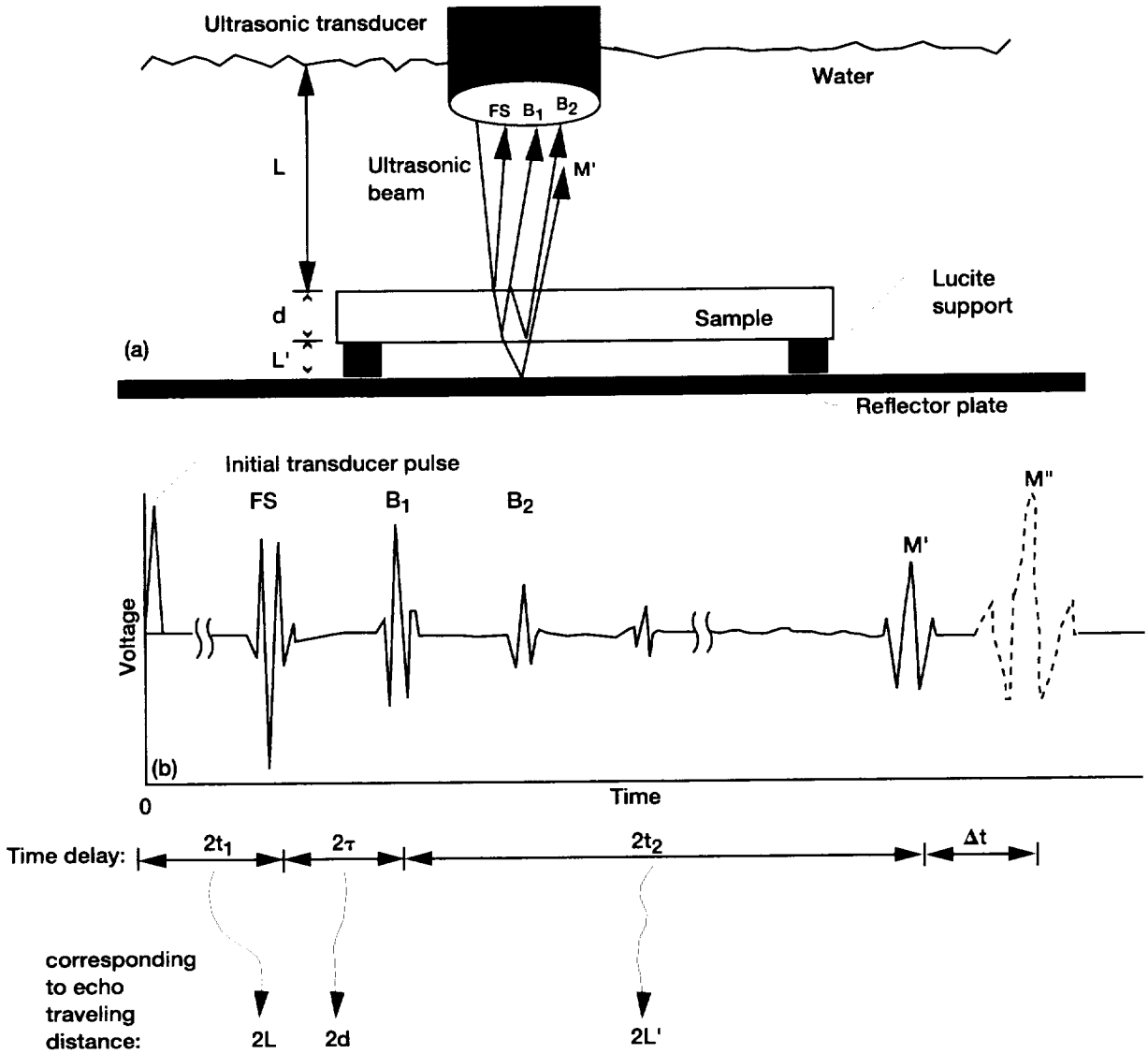

Figure 2.—Ultrasonic pulse-echo immersion testing. (a) Schematic of ultrasonic pulse-echo immersion testing. (b) Resulting waveforms.

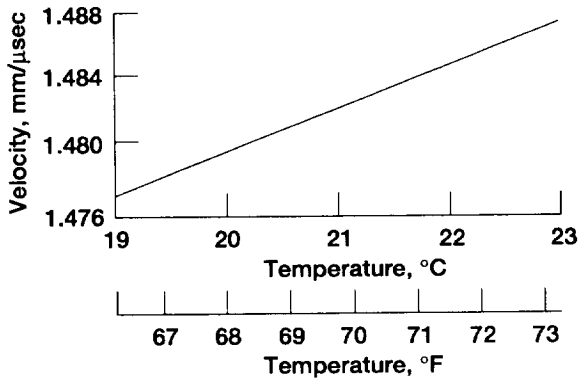

Figure 3.—Velocity of water versus temperature from ref. 1. $C = (1410 + 4.21T - 0.037T^2) \times 10^{-3}$ where C = water velocity (mm/μsec) and T= water temperature (°C).

The thickness (d) of the sample can be determined from:

$$d = \tau V \tag{7}$$

Substituting Eq. (7) into Eq. (6) gives:

$$\Delta t = \frac{2\tau V}{c} - 2\tau \tag{8}$$

Rearranging Eq. (8) gives:

$$V = c\left(\frac{\Delta t}{2\tau} + 1\right) \tag{9}$$

As for conventional velocity measurements, 2τ is experimentally obtained from the pulse-echo time delay between the first front surface (FS) and first back surface (B1) echoes, or between 2 successive back surface echoes (such as B1 and B2 [Fig. 2]). Δt is the pulse-echo time difference between the first echo off the reflector plate front surface with and without the sample present, respectively. Water velocity (c) can be determined in the pulse-echo configuration by recording the times (t_{wi}) where ultrasonic echo peaks occur for 2 height (Z_i) positions of the transducer and calculating:

$$c = \frac{2(Z_1 - Z_2)}{t_{w1} - t_{w2}} = \frac{2(\Delta Z)}{\Delta t_w} \tag{10}$$

Alternately, water velocity (c) can be calculated from (Ref. 1):

$$c(mm/\mu\,\text{sec}) = (1410 + 4.21T - 0.037T^2) \times 10^{-3} \tag{11}$$

where T is temperature in °C. Figure 3 shows a plot of water velocity (c) versus temperature.

As seen from Eq. (9), sample thickness (d) is not a variable in the equation. Thus, this method does not require prior knowledge of sample thickness and if extended to multiple measurements across the sample (imaging), sample thickness variation effects are eliminated in the image.

ERROR IN THICKNESS-INDEPENDENT VELOCITY MEASURE

The precision (uncertainty) in the thickness-independent velocity (σ_V) due to the random errors in the measurements of the variables Δt, 2τ, Δt_{wi}, and ΔZ was obtained by use of Eqs. (9) and (10) and the variance relation (Ref. 8) to give:

$$\sigma_V^2 = \left(\frac{\partial V}{\partial(\Delta t)}\right)^2 (\sigma_{\Delta t})^2 + \left(\frac{\partial V}{\partial(2\tau)}\right)^2 (\sigma_{2\tau})^2 + \left(\frac{\partial V}{\partial(\Delta t_{wi})}\right)^2 (\sigma_{\Delta t_{wi}})^2 + \left(\frac{\partial V}{\partial(\Delta Z)}\right)^2 (\sigma_{\Delta Z}) \tag{12}$$

where $\sigma_{\Delta t}$, $\sigma_{2\tau}$, $\sigma\Delta t_{wi}$ and $\sigma_{\Delta Z}$ are the uncertainties in measuring: the time difference between the first echo off the reflector plate front surface with and without the sample present, the time delay between the first front surface (FS) and first back surface (B1) echoes (or between 2 successive back surface echoes), the time difference between the two ultrasonic echo peaks that occur at two height positions of the transducer, and the positional difference between two height positions of the transducer, respectively. Percent uncertainty in the thickness-independent velocity is given by

$$U_V = \left(\left|\frac{\sigma_V}{V}\right|\right)100 \tag{13}$$

Using typical values of Δt = 3 μsec, 2τ = 0.5 μsec, Δt_{wi} = 6.8 μsec and ΔZ = 0.25 cm, Fig. 4(a) shows percent uncertainty in the thickness-independent velocity (U_V) as a function of uncertainties in measuring echo time difference ($\sigma_{\Delta t} = \sigma_{2\tau} = \sigma_{\Delta t_{wi}}$) and transducer positional difference ($\sigma_{\Delta Z}$). Noting that the uncertainty in measuring echo time difference can be expressed in terms of the experimental analog-to-digital sampling rate (SR) according to:

$$\sigma_{\Delta t} = \sigma_{\Delta 2\tau} = \sigma_{\Delta t_{wi}} = \left(\frac{1}{2 * SR}\right), \tag{14}$$

Fig. 4(b) shows percent uncertainty in the thickness-independent velocity (U_V) as a function of sampling rate (SR) and uncertainty in measuring transducer positional difference ($\sigma_{\Delta Z}$). It can be seen from Fig. 4 that the U_V is less than 1 percent for reasonable sampling rates (≥100 MHz) and reasonable uncertainty in measuring echo time (≤0.005 μsec) and transducer positional differences (≤10 μm).

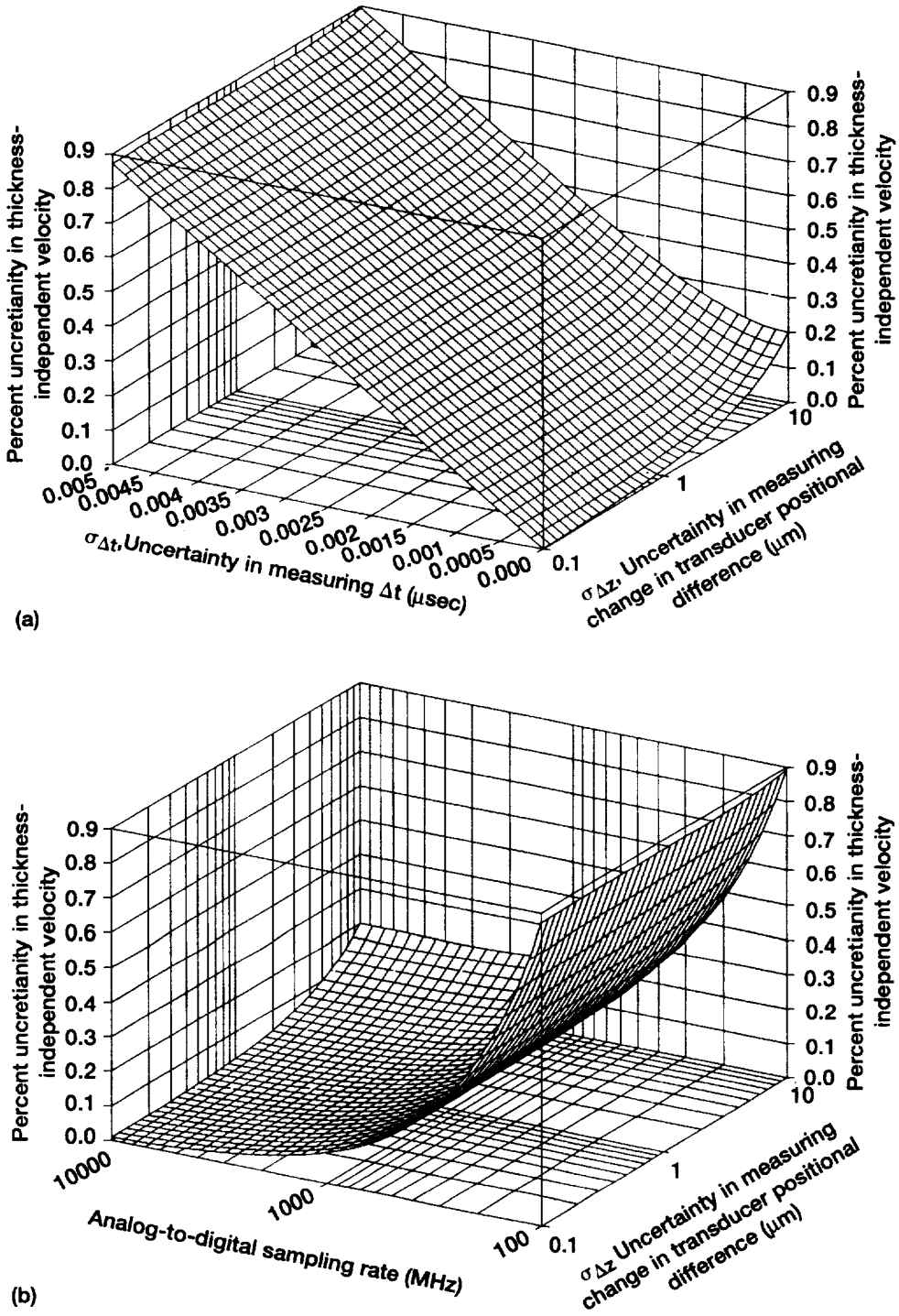

Figure 4.—Percent uncertainty in thickness-independent velocity. (a) Percent uncertainty in thickness-independent velocity as a function of uncertainties in measuring changes in time and transducer positional difference. (b) Percent uncertainty in thickness-independent velocity as a function of analog-to-digital sampling rate and uncertainty in measuring change in transducer positional difference.

The accuracy (vicinity to true value) in the thickness-independent velocity is the result of both random error identified above plus the systematic error caused by diffraction effects. The latter is estimated to be ~0.5 percent for the experimental setup of this investigation where unfocused transducers were utilized (see Appendix).

EXPERIMENTAL

Materials.—The specimens ultrasonically imaged were several monolithic silicon nitride ceramic disks, a silicon nitride wedge, a metal matrix composite (MMC) sample, and a polymer matrix composite (PMC) panel. The ceramic disks were 2 to 4±0.005 mm thick and 40 mm in diameter and contained 6 distinct areas of higher-than-average (HTA) pore fraction located 60° apart (Fig. 5). They also contained a pore fraction gradient from edge to center. The ceramic wedge was machined to provide a 0.300 mm edge-to-edge thickness gradient (lengthwise). The ceramic wedge contained 3 areas of HTA pore fraction and a pore fraction gradient from edge-to-center. The MMC panel was several plies thick with continuous alumina fibers in an aluminum matrix. It contained unspecified major fiber volume fraction variations and varied in thickness from ~2.4 to 2.7 mm (~0.300 mm thickness variation) lengthwise over the entire sample. The panel was ~4 by 15 cm in lateral dimensions. The PMC panel was 12-ply unidirectional with continuous graphite fibers in a polyimide matrix. It contained a 10 percent fiber volume fraction variation and an ~60 μm thickness variation in a 5 by 5 cm central region.

General Set-up For The Thickness-independent Reflector Plate (TIRP) Velocity Imaging.—For the ceramic materials, 20 MHz unfocused and 50 MHz focused transducers with 3 mm element diameter and 12.5 mm focal length were used for scanning. For the MMC panel, focused 10 MHz transducer with 9.5 mm element diameter and 76 mm focal length, and focused 30 MHz transducer with 6 mm element diameter and 19 mm focal length, were used for scanning. For the PMC sample, a focused 3.5 MHz wave transducer with 12.5 mm element diameter and 50 mm focal length was used for scanning. All transducers were of the longitudinal wave type. The time difference between 2 successive back surface echoes B1 and B2, and between the reflector echoes M' and M'', were used for 2τ and Δt, respectively (Fig. 2). A cross-correlation computer algorithm (Ref. 9) was used to calculate 2τ and Δt, and velocity was subsequently calculated using Eq. (9). Phase relationships were examined for 1) $B1$ compared to $B2$ and 2) M' compared to M''. If echoes were in-phase with respect to each other, the time occurrence of the *maximum* in the correlation function was used to calculate time delay. If the echoes were phase-inverted, the time occurrence of the minimum in the correlation function was used to calculate time delay.

Tungsten sheet of thickness equal to 0.159 cm (1/16 in.) was used as the reflector plate because tungsten has an acoustic impedance ~70 times higher than water, resulting in the highest possible reflection echo amplitude

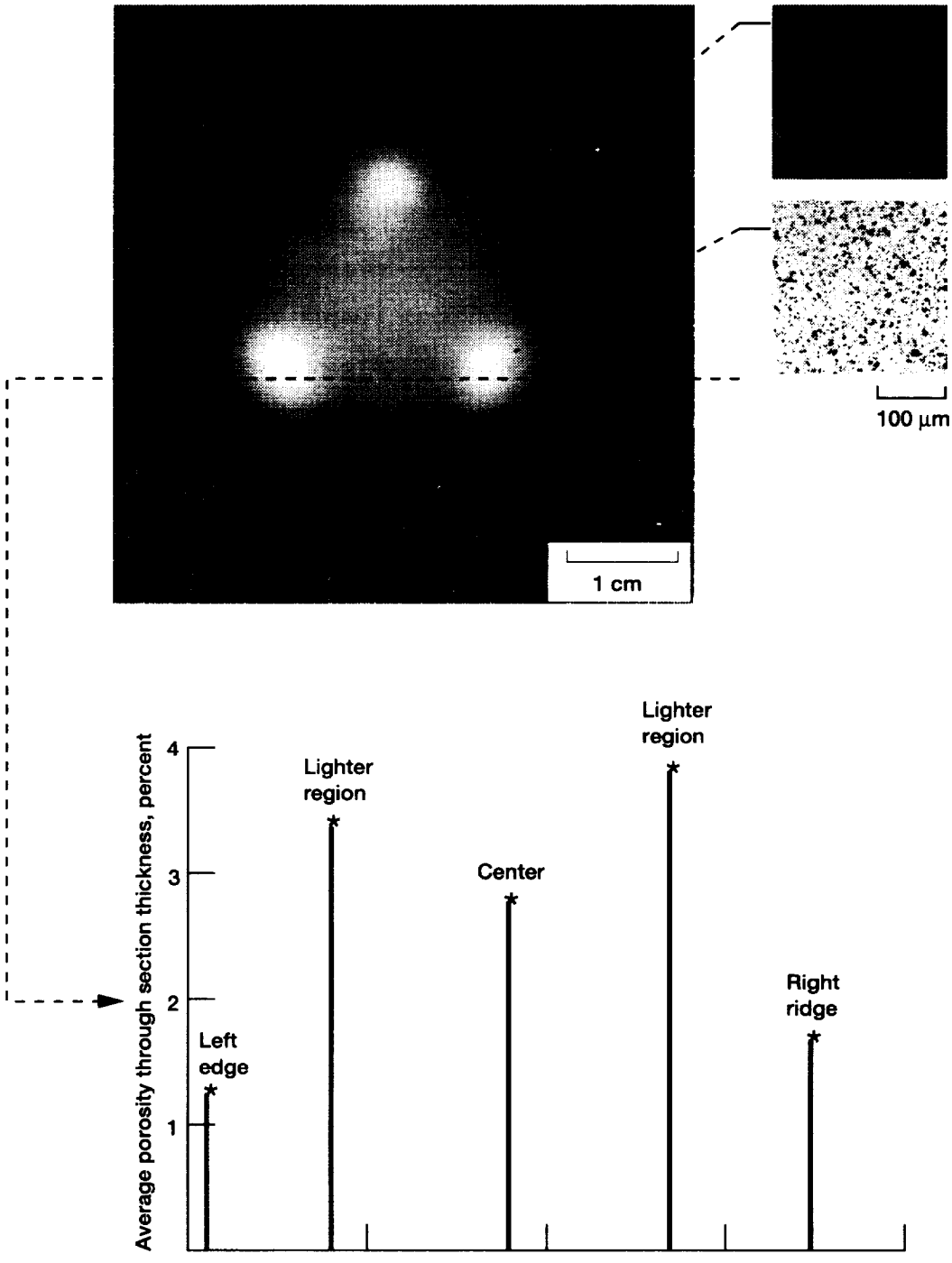

Figure 5.—Silicon nitride ceramic disk containing higher-than-average pore fraction areas and edge-to-center density gradient.

of any reflector plate material. The sample to be scanned was placed on plastic supports of thickness equal to 1.27 cm (0.5 in.) sitting on the reflector plate. The supports were placed so they were as unobtrusive as possible with regards to sample contact since ultrasonic waves needed to pass through the sample to the reflector plate for an entire sample to be scanned.

After the sample was placed on the supports, pulser-receiver gain and/or attenuation settings and voltage amplifier settings were adjusted so that echoes off the sample surfaces and the reflector plate were visible. Transducers were positioned (defocused off sample front surface) above the sample at distances where highest back surface echo B1 amplitude was present. As an example, for the 20 MHz unfocused transducer interrogating the ceramic materials, the transducer-to-sample distance was ~4 cm. (It is critical not to confuse the echoes off the reflector plate with the second set of echoes originating from the front surface and back surface of the sample when executing the TIRP velocity imaging method. The methodology for avoiding confusion is to raise and lower the sample off the supports while noting the time position of the stationary echo train associated with the stationary reflector plate. Additionally, the second set of echoes originating from the front and back surface of the sample will always occur at twice the delay time where the first set of those echoes occurs. As an example, if the first set of sample echoes begins at 50 μsec time position, the second set will begin at 100 μsec. It has been found that if the water path between the reflector plate and an ~3 mm thick sample is ~1.27 cm (0.5 in.), the first echo off the reflector plate front surface will occur at ~20 μsec after the time where the first set of sample echoes originates.)

Prototype System Configuration for TIRP Imaging.—The prototype was a VAX/IEEE-GPIB-controlled scan system originally built for contact scans but modified for immersion mode for this investigation. The reader is referred to Ref. 10 for more detail on the instrumentation used in this system. Two scans were required to execute the TIRP velocity imaging method. In the first scan, echoes $B1$, $B2$ and M' were acquired by time windowing and digitizing individual echoes. A programmable time synthesizer allowed sequential windowing at the correct time location of each echo. In the second scan, the sample was removed and M" was acquired. The prototype analog-to-digital (A/D) converter had bandwidth capability greater than 1 GHz (200 to 500 MHz sampling rates were used) and 9-bit digital dynamic range. A recirculating constant temperature bath was employed to keep the temperature of a small water bath (0.003785 m^3 [1 gallon]) constant within ±0.3 °C. A 1 mm-scan increment was used in the scans obtained with the prototype TIRP system. Images are shown with 255 discrete levels of gray scale that appear continuous to the eye.

(A "slant correction" procedure was required before the scan to account for nonlevelness in the set-up [which outweighed thickness variations in the samples tested] so that echoes would remain ~ centered in time windows throughout the scan. The slant correction procedure (1) allowed the maximum time resolution of

individual echoes without losing any part of the time domain waveform and (2) negated the need for specialized leveling equipment. This procedure was started by placing the transducer at the proper height above the sample and positioning it at the left-most portion of the scan. The transducer was then moved over the extent of the sample four separate times in the left-to-right (x-) direction. Each movement corresponded to one of echoes $B1$, $B2$, M', and M'' being kept centered in the time window via time synthesizer manual adjustment (Ref. 10). Then, the transducer was positioned at the bottom-most portion of the scan and the procedure repeated for the four echoes with the transducer moved in the bottom-to-top (y-) direction. In each case, the total time adjustment required to keep the echo centered was noted which allowed the calculation of eight "slant correction factors" [nsec/μm] total in the x- and y- directions. The slant correction factors were placed into scanner control software so that during the windowing of the echo during the scan, the echo was automatically repositioned to stay ~ centered within the oscilloscope time window throughout the whole scan.)

Sonix System Configuration For TIRP Imaging.—The Sonix, Inc. system used was a 486/33 MHz PC-AT-controlled scan system. A large water bath (≥0.3785 m^3 [100 gallons]) was present not requiring temperature regulation. An A/D converter having 100 MHz bandwidth and 8-bit digital dynamic range was employed. 800 MHz effective sampling rate obtained using the Sonix Equivalent Time Sampling (ETS) algorithm (Ref. 11) was required to obtain accurate TIRP images on the Sonix system. (It is recommended to use an A/D converter with true 1 GHz sampling rate so that the ETS algorithm is not needed. Such a converter is commercially available from Sonix.) The Sonix implementation of TIRP velocity imaging required 3 scans to acquire the waveform data (Ref. 7). (The Sonix c-scan system is 100x faster than the prototype system so the extra scan required as compared to the prototype method was not a significant issue.) B1 and B2 were acquired in the first scan. M' was acquired in the second scan. M" was acquired in the third scan after removing the sample. To account for sample nonlevelness, the front surface follower gate feature (Ref. 11) was applied in the scan where B1 and B2 were acquired and the data gates (Ref. 11) were made as long as required during the scans where the reflector echoes M' and M" were acquired. 0.5 and 1 mm scan increments were used in the scans. Images are shown with 248 discrete levels of gray scale that appear continuous to the eye.

Additional Imaging.—Additional images were obtained using the Sonix system for comparison with TIRP velocity images. Peak amplitude c-scan images where the echo off the specimen back wall was gated were obtained using 0.25 scan increment. *Apparent* velocity images were obtained as calculated using Eq. (3) with a single value for thickness (d). The thickness value was an average value obtained from several measurements at different sample locations. Scan increments of 0.5 and 1 mm were used for scans where *apparent* velocity images were obtained. Please note that that *apparent* velocity and c-scan time-of-flight maps will be affected similarly by thickness variations, so only the apparent velocity images are shown.

RESULTS

Prototype versus Sonix System Configuration TIRP Images.—Figures 6(a) and (b) show TIRP images of one of the uniformly-thick silicon nitride disks obtained with the prototype and Sonix systems, respectively. The disk was scanned with the same 20 MHz unfocused transducer in both cases. The prototype image was smoothed while the Sonix system image was low-pass filtered and then smoothed. Note that the images are nearly identical qualitatively (in revealing the 6 higher-than-average [HTA] pore fraction areas) and quantitatively (the range of velocity values is nearly identical [maximum - minimum value ~2 to 3 percent]). The imaging method was thus validated on two ultrasonic systems having different instrumentation and control/data acquisition methods.

Peak Amplitude C-scan and Apparent Velocity Images versus TIRP Velocity Image.—Figure 7 shows imaging results for the silicon nitride ceramic wedge with the 0.300 mm edge-to-edge thickness gradient (lengthwise), 3 areas of HTA pore fraction and an edge-to-center pore fraction gradient. Figure 7(a) shows for the wedge a 50 MHz focused peak amplitude c-scan image where the back wall was gated (0.25 mm scan increment). Figure 7(b) shows a 20 MHz unfocused *apparent* velocity image (0.5 mm scan increment). Figure 7(c) shows a 20 MHz unfocused TIRP velocity image (0.5 mm scan increment). The peak amplitude c-scan image (Fig. 7(a)) does not reveal the thickness or microstructural variations. This is likely due to the fact that the attenuation coefficient at ~50 MHz in silicon nitride (even with some porosity) is extremely low such that a system with 8-bit digital dynamic range cannot resolve it. The *apparent* velocity image (Fig. 7(b)) shows an ~10 percent velocity variation from top-to-bottom edge; some microstructural variation is evident but is mostly masked by the thickness variation. In this image, the HTA pore fraction area at the top of the disk is accentuated while the lower HTA pore fraction area is masked totally by the thickness gradient. In the TIRP velocity image (Fig. 7(c)), the lower HTA pore fraction area is revealed, the top HTA area is de-emphasized, and an ~4 percent total velocity variation is seen. By eliminating the effects of thickness from the ultrasonic image, the TIRP method accurately quantified (in terms of velocity variation) the pore fraction variations that were *not* revealed in the peak amplitude c-scan image and incorrectly represented in the conventional velocity image for this ceramic material.

Figure 8 shows imaging results for the MMC panel containing fiber volume fraction variations and a 0.300 mm edge-to-edge thickness gradient (lengthwise). Figures 8(a) and (b) show for the panel 10 and 30 MHz peak amplitude c-scan images where the back wall was gated (0.25 mm scan increment). Figure 8(c) shows an *apparent* velocity image (1 mm scan increment) obtained at 10 MHz. Figure 8(d) shows a TIRP velocity image (1 mm scan increment) obtained at 10 MHz. The 10 MHz peak amplitude c-scan image (Fig. 8(a)) reveals alternate light and dark bands that may indicate continuous fibers and also indicates the discrete steps of the varying fiber

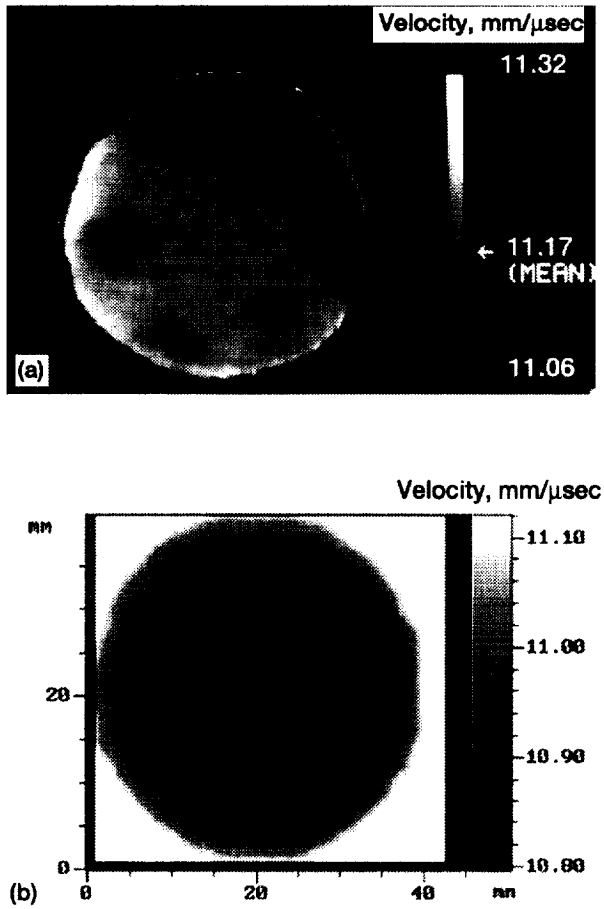

Figure 6.—Thickness-independent velocity images of silion nitride disk obtained from lab-based prototype system and Sonix, Inc. C-scan system implementation. (a) Image obtained from prototype system. (b) Image obtained from Sonix system. 20 MHz unfocused transducer was used for scans.

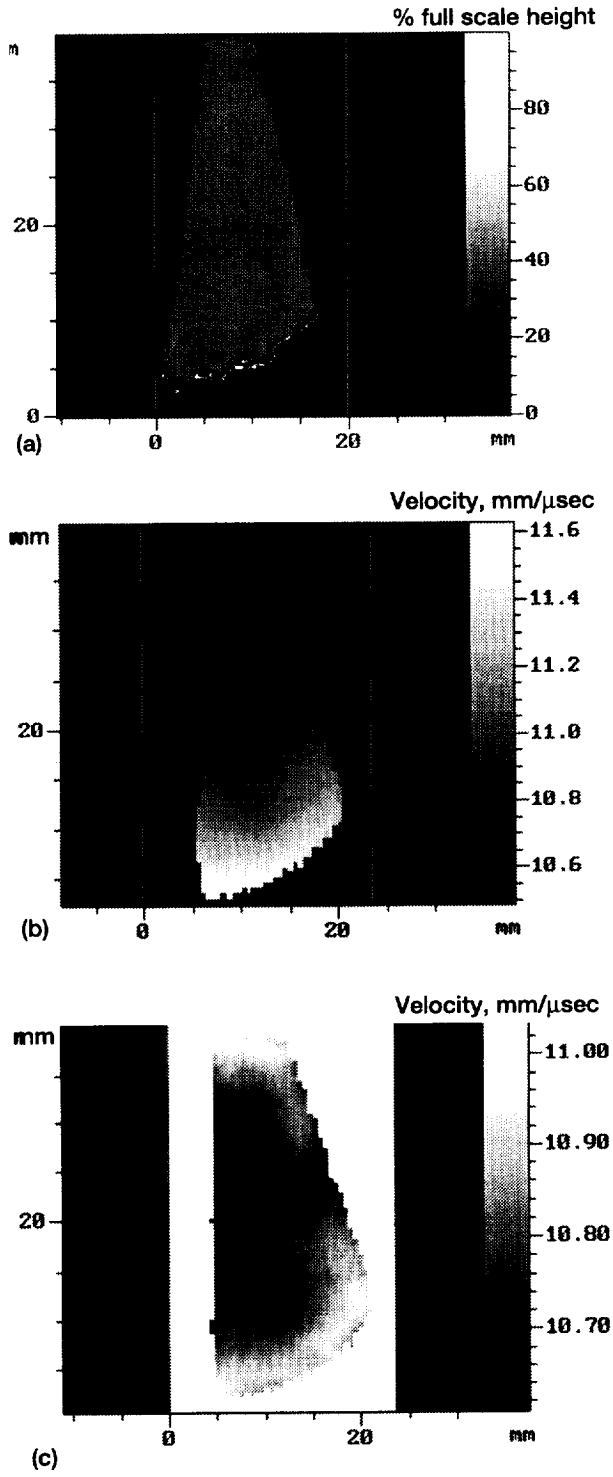

Figure 7.—Ultrasonic images of silicon nitride wedge having pore fraction variations and a 300 μm thickness gradient edge-to-edge (lengthwise). (a) C-scan peak amplitude image where back wall echo was gated, 50 MHz. (b) Apparent velocity image, 20 MHz. (c) Thickness-independent velocity image, 20 MHz.

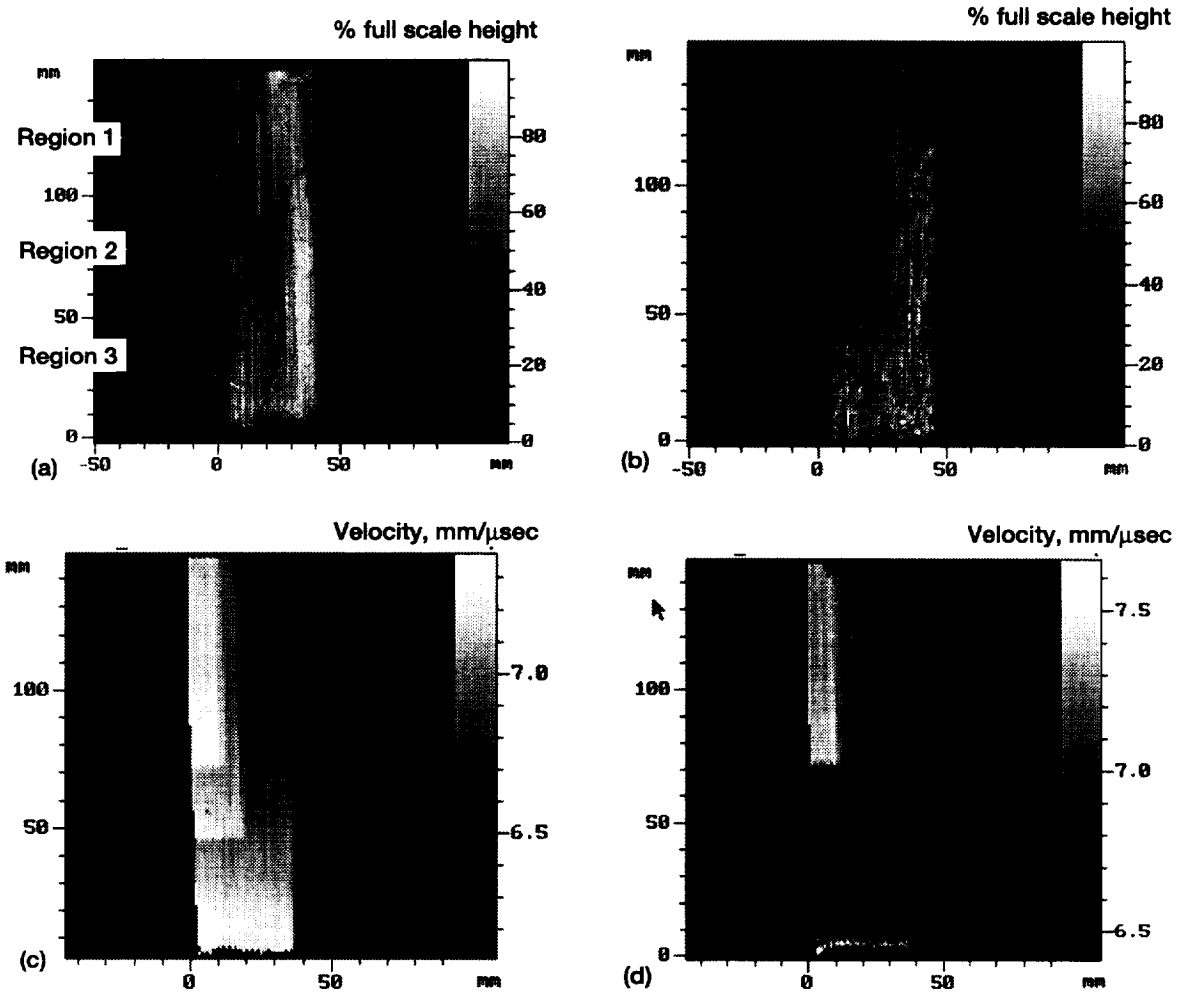

Figure 8.—Ultrasonic images of MMC panel having fiber volume fraction variations and a 300 μm thickness gradient edge-to-edge (lengthwise). (a) C-scan peak amplitude image where back wall echo was gated, 10 MHz. (b) C-scan peak amplitude image where back wall echo was gated, 30 MHz. (c) Apparent velocity image, 10MHz. (d) Thickness-independent velocity image, 10MHz.

volume fraction regions resulting from manufacture. However, no discernible gray variations are indicated between the three regions that would indicate significantly different microstructure between the steps. In contrast, the 30 MHz peak amplitude c-scan image (Fig. 8b) shows a major gray difference indicating fiber volume fraction differences between region 3 and the other two regions. A gray difference between regions 1 and 2 is still not resolvable. The 30 MHz peak amplitude c-scan being more revealing than the 10 MHz c-scan is consistent with the fact that a greater amount of scattering and/or absorption occurs as frequency is increased. Thickness variation was not revealed in these peak amplitude c-scan images. Most likely this was because it was not large enough to cause significant attenuation at 10 to 30 MHz to be resolved with 8-bit digital dynamic range. The *apparent* velocity image (Fig. 8(c)) very clearly reveals the three regions' microstructural differences but also incorrectly indicates due to thickness variation that the bottom of the panel is ~ the same velocity as region 1. The TIRP velocity image (Fig. 8(d)) most clearly reveals the regions' microstructural differences and also shows that the bottom of the panel is 10% lower in velocity than region 1. By eliminating the effects of thickness from the ultrasonic image, the TIRP method accurately quantified (in terms of velocity variation) the fiber volume fraction variations that were *not* revealed in the 10 MHz peak amplitude c-scan image, only partially revealed in the 30 MHz peak amplitude c-scan image, and incorrectly quantified in the conventional velocity image for this MMC material. It is important to note that the peak amplitude c-scan images appear to resolve individual fibers while the TIRP and conventional velocity images do not. Thus the TIRP method is most applicable to accurate global microstructural variation as opposed to discrete feature/defect characterization.

Figure 9 shows imaging results for the PMC sample containing 10 percent fiber volume fraction variations and a 60 μm thickness variation over a 5 by 5 cm area. Figure 9(a) shows for the 5 by 5 cm area a peak amplitude c-scan image where the back wall was gated (0.25 mm scan increment). Figure 9(b) shows an *apparent* velocity image (1 mm scan increment). Figure 9(c) shows a TIRP velocity image (1 mm scan increment). All scans were performed using a 3.5 MHz focused transducer. The peak amplitude c-scan image (Fig. 9(a)) shows gray scale variation including 2 darker-than-average (low amplitude) indications near the center. These darker regions were found to have on average 10 percent lower fiber volume fraction than that of surrounding regions after metallographic preparation followed by optical image analysis. The *apparent* velocity image (Fig. 9(b)) shows approximately the same gray scale variation as the c-scan image. The TIRP velocity image (Fig. 9(c)) shows increased contrast between light and dark areas as compared to the *apparent* velocity image due to the elimination of thickness effects. Approximately 10 percent velocity variation is indicated in this region. The redistribution of velocity values after elimination of thickness variation effects is shown in the histograms of Figs. 9(d) and (e). For this PMC material, the TIRP method confirmed and accurately quantified (in terms of velocity variation) the fiber volume fraction variations seen in the peak amplitude c-scan image.

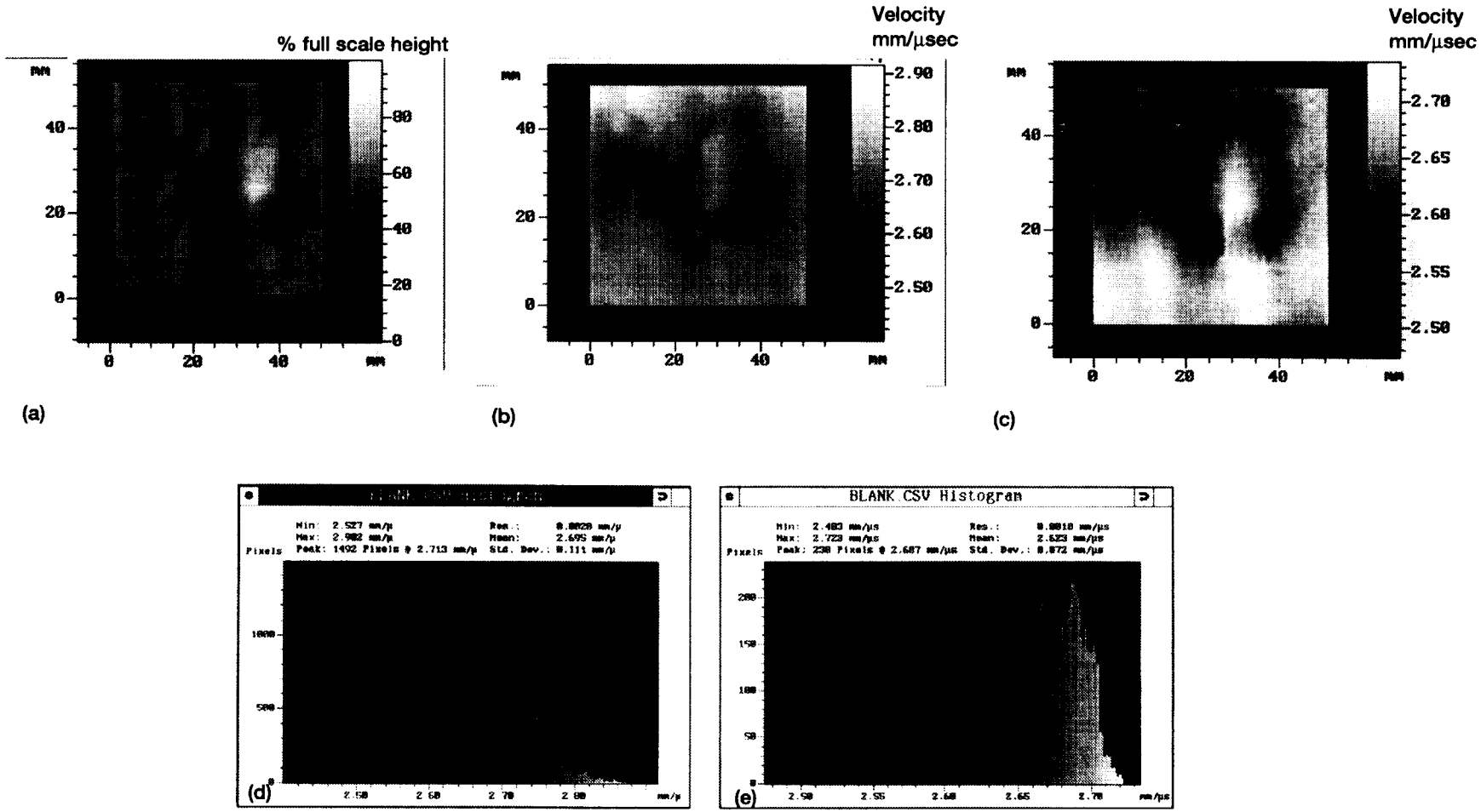

Figure 9.—Ultrasonic imaging results for polymer matrix composite sample area having 10% fiber volume fraction variations and a 60 μm thickness variation. 3.5 MHz transducer was used for scans. Also shown are histograms of velocity images. (a) C-scan peak amplitude image where back wall echo was gated. (b) Apparent velocity image. (c) Thickness-independent velocity image. (d) Histogram of velocity values for apparent velocity image. (e) Histogram of velocity values for thickness-independent velocity image.

DISCUSSION: EFFECT OF FLUID TEMPERATURE

Viewing Eqs. (9) and (11), it would appear that even minor variations in fluid temperature would have a major effect on the velocity obtained for a material. To investigate the effect of fluid temperature on velocity in silicon nitride, an experiment was performed several times in which 2τ (the pulse-echo time delay between B1 and B2) and Δt (the pulse-echo time difference between the first echo off the reflector plate front surface with and without the sample present, respectively) from Eq. (9) were obtained at 15.6 to 32.2 °C (60 to 90 °F) in increments of 2.77 °C (5 °F) at a point on the silicon nitride disk. Water velocity (c) was calculated according to Eq. (11). Velocity in silicon nitride was then calculated as a function of temperature according to Eq. (9). Table I and Fig. 10 show a typical result from the experiments. The following results were seen with respect to increasing the temperature from 15.6 to 32.2 °C according to the precision available: water velocity increased ~2.7 percent, Δt decreased ~2.8 percent, 2τ remained constant (0.482 μsec), and velocity in silicon nitride remained nearly constant (varied in an unpredictable fashion by only 0.74 percent, at least a portion of which was likely due to the random error in the measurement of the variables in Eq. (9) as discussed earlier). To understand the almost exact offsetting changes between Δt and water velocity, note that Eq. (6) when rearranged can be used to predict water velocity (c) as function of Δt:

$$c = \frac{2d}{(\Delta t + 2\tau)} \tag{15}$$

Using Eq. (15), Substituting the values of silicon nitride disk thickness (d) equal to 0.2619 cm and 2τ equal to 0.482 μsec, and plotting predicted water velocity (c) versus Δt for the range of Δt values seen experimentally, the result is shown in Fig. 11. It can be seen that over the temperature range (15.6 to 32.2 °C [60 to 90 °F]) corresponding to this range of Δt values, predicted water velocity (c) is inversely proportional to Δt in a highly linear manner and the ratio of the predicted *percentage change* in water velocity over the *percentage change* in Δt is ~−1. This result helps explain the offsetting changes between Δt and water velocity seen experimentally. The overall result of this experiment indicates very little temperature-dependence of velocity in silicon nitride between 15.6 to 32.2 °C (60 to 90 °F).

From a practical standpoint, it is still important to keep temperature nearly constant during the scan procedure. First, other materials may exhibit more significant change in velocity with temperature than does silicon nitride leading to masking (or accentuation) of microstructural variation if fluid temperature varies. Secondly, most ultrasonic imaging systems including the two used in this investigation implement a windowing or gating procedure to isolate and digitize individual ultrasonic echoes. The windows or gates are usually a time extent just large enough to envelope the echo for maximum digital resolution or to reduce calculation time. If temperature varies during the

TABLE I.—RESULTS OF INVESTIGATION OF EFFECT OF WATER TEMPERATURE ON VARIABLES IN EQUATION (9)

Temperature, °F (±0.1°F)	Temperature, °C (±0.1 °C)	Water velocity, mm/μsec (±0.005 mm/μsec)	2τ, μsec (±0.001 μsec)	Δt, μsec (±0.001 μsec)	Silicon nitride velocity, mm/μsec (±0.01 mm/μsec)
60	15.5	1.466	0.482	3.066	10.79
65	18.3	1.474	0.482	3.057	10.82
70	21.1	1.482	0.482	3.050	10.86
75	23.8	1.489	0.482	3.028	10.84
80	26.6	1.495	0.482	3.014	10.85
85	29.4	1.501	0.482	3.005	10.86
90	32.2	1.507	0.482	2.98	10.82

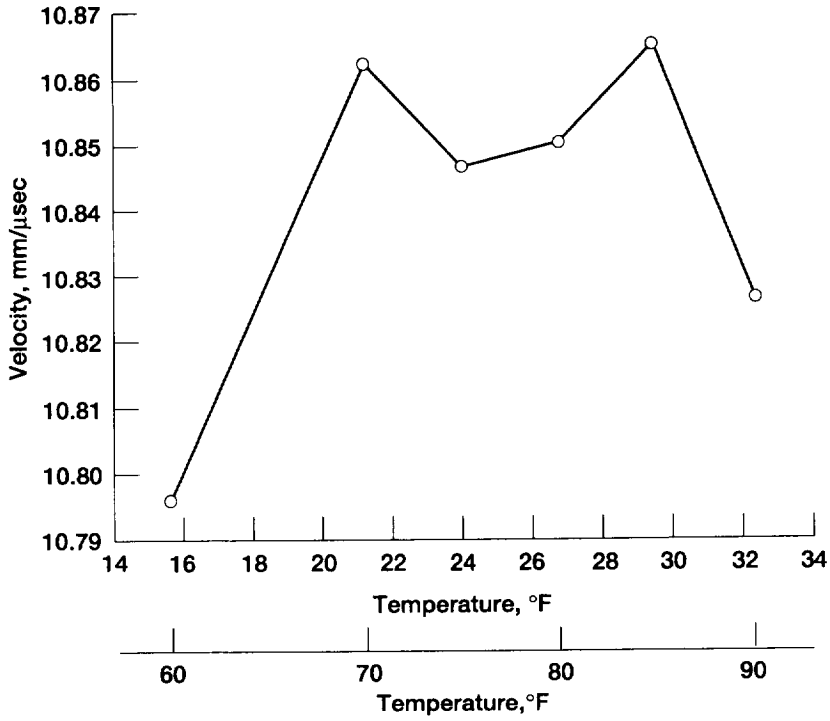

Figure 10.—Velocity versus temperature for silicon nitride sample. Error in velocity measurement ~0.01 mm/μsec.

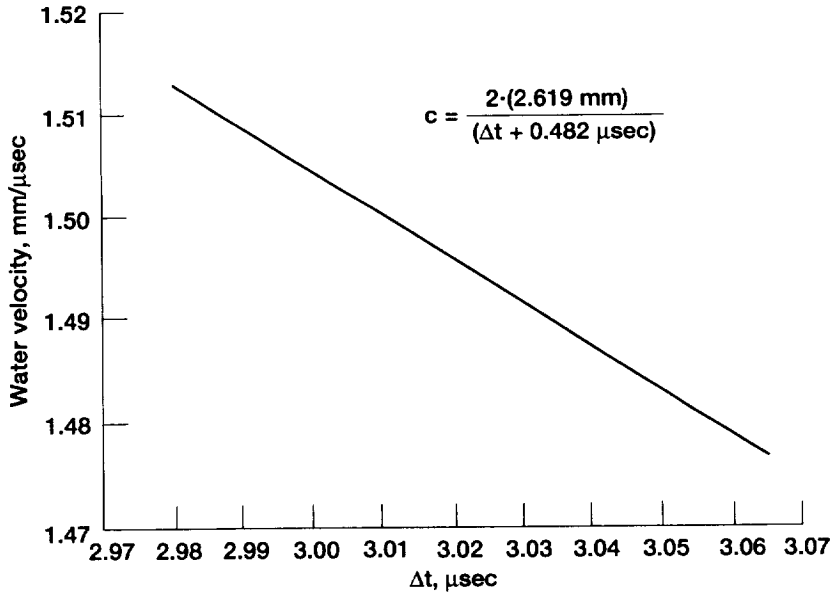

Figure 11.—Water velocity (c) versus Δt as predicted from Eq. (15). Disk thickness (d) = 2.619 mm and 2τ = 0.482 μsec.

scan procedure, the echoes off the reflector plate front surface with and without the sample present will move out of the gate extent (i.e., t' and t'' will vary [see Eqs. (4) and (5)]) (Fig. 12), and digitizations containing incomplete echoes will result leading to invalid velocity values. For temperature control, it is suggested to use a large water tank ($\geq$0.3785 m^3 [100 gal]) that due to its capacity is slow to respond to ambient temperature changes. A recirculating constant temperature bath is recommended for use with smaller tanks such as those used in tabletop or lab-based scan systems.

SUMMARY AND SIGNIFICANCE

This article described a single transducer ultrasonic imaging method that eliminates the effect of plate thickness variation in the image, i.e., is thickness-independent. The method thus isolates ultrasonic variations due to material microstructure. Its use can result in significant cost savings because the ultrasonic image can be interpreted correctly without the need for machining to achieve precise thickness uniformity during nondestructive evaluations of material development. The method is based on measurement of ultrasonic velocity and is precise to less than 1 percent using conditions of this investigation.

The thickness-independent imaging method was validated on two ultrasonic systems having different instrumentation and control/data acquisition methods. Images obtained using the thickness-independent methodology were compared with apparent velocity maps and c-scan echo peak amplitude images for monolithic ceramic (silicon nitride), metal matrix composite (MMC), and polymer matrix composite (PMC) materials having thickness and microstructural variations. It was found that peak amplitude c-scans were not visibly affected by the up to 300 mm thickness variation in these materials. Additionally, the peak amplitude c-scans did not clearly reveal the microstructural variations in these materials. However, apparent velocity images indicating time-of-flight variations showed significant superposition of thickness effects which skewed the true picture of material microstructure. By eliminating the effects of thickness from the ultrasonic image, the method (1) accurately quantified (in terms of velocity variation) the pore fraction variations that were *not* revealed in the peak amplitude c-scan image and incorrectly represented in the conventional velocity image for a ceramic material, (2) accurately quantified the fiber volume fraction variations that were only partially revealed in a peak amplitude c-scan image and incorrectly quantified in the conventional velocity image for an MMC material and (3) highlighted and accurately quantified the fiber volume fraction variations originally detected in the peak amplitude c-scan image for a PMC material. The thickness-independent method, currently being commercialized under a cooperative agreement between NASA Lewis Research Center and Sonix, Inc, has applicability to inspection of some complex shapes such as hollow tubes as indicated in Ref. 5.

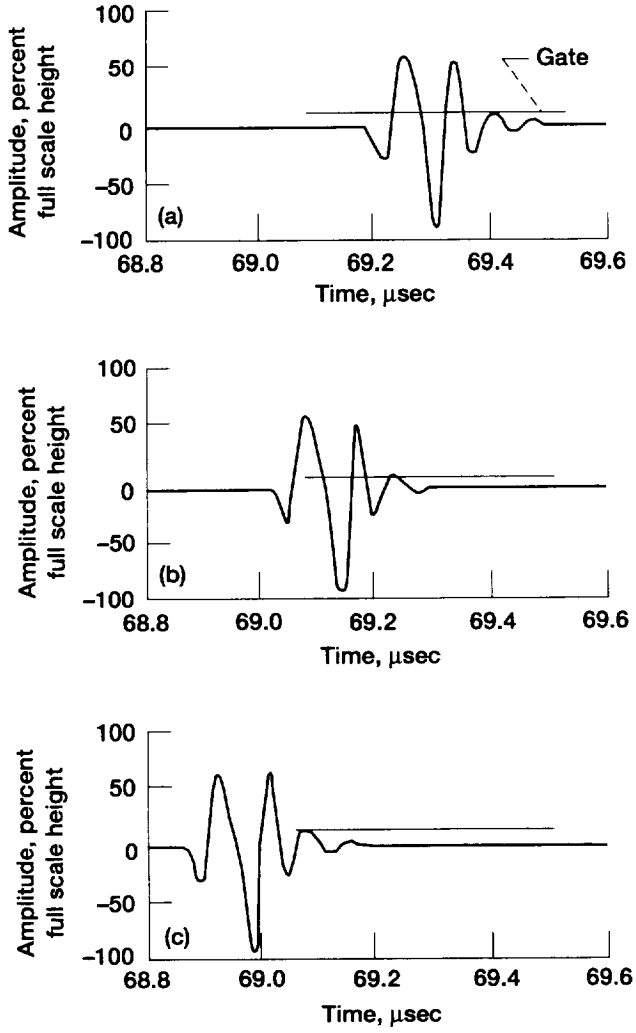

Figure 12.—Ultrasonic echo position as a function of temperature for M", the first echo off the reflector plate front surface with the sample removed. (a) Echo position at 22.2 °C (72 °F). (b) Echo position at 23.3 °C (74 °F). (c) Echo position at 24.4 °C (76 °F).

REFERENCES

1. Nondestructive Testing Handbook, second edition, Volume 7 Ultrasonic Testing, eds. Birks, A.S., Green, R.E., and McIntire, P. American Society For Nondestructive Testing, 1991, pp. 227–230, 387–390, 405, 225.
2. Bashyam, M.: Thickness Compensation and Dynamic Range Improvement For Ultrasonic Imaging of Composite Materials. Proc. Of the 17th Annual Review of Progress in Quantitative Nondestructive Evaluation, La Jolla, CA, July 15–20, 1990. Vol. 10A. Plenum Press, 1991, pp. 1035–1042.
3. Roth, D.J., et. al.: An NDE Approach For Characterizing Quality Problems in Polymer Matrix Composites. Proc. 40th International SAMPE Symposium, Anaheim, CA, May 8–11, 1995, pp. 288–299.
4. Hsu, D.K., et. al.: Simultaneous determination of ultrasonic velocity, plate thickness and wedge angle using one-sided contact measurements. NDT&E International 1994 Volume 27, Number 2, pp. 75–82.
5. Sollish, B. D.: Ultrasonic Velocity and thickness gage, United States Patent No. 4,056,970, Nov. 8, 1977.
6. Pichè, L.: Ultrasonic velocity measurement for the determination of density in polyethylene. Polymer Engineering and Science, Vol. 24, No. 17, Mid-December 1984, pp. 1354–1358.
7. Roth, D. J., et. al.: Commercial Implementation of Ultrasonic Velocity Imaging Methods via Cooperative Agreement Between NASA - Lewis Research Center and Sonix, Inc. NASA TM–107138, 1996.
8. Bevington, R. P., Data Reduction and Uncertainty Analysis for the Physical Sciences, Chapter 4, 1969. McGraw-Hill, New York, NY.
9. Hull, D.R.; Kautz, H.E.; and Vary, A.: Measurement of Ultrasonic Velocity Using Phase-Slope and Cross-Correlation Methods. Mater. Eval., vol. 43, no. 11, 1985, pp. 1455–1460.
10. Roth, D.J., et. al.: Quantitative Mapping of Pore Fraction Variations in Silicon Nitride Using an Ultrasonic Contact Scan Technique. Res. Nondestr. Eval., vol. 6, 1995, pp. 125–168.
11. Ultrasonic C-scan Users Guide, V3.10d, January, 1995. Sonix, Inc. 8700 Morrissette Drive, Springfield, VA 22152.

APPENDIX—EFFECTS OF DIFFRACTION (BEAM SPREAD)

In the reflector plate methodology of this experiment, the transducer is separated from the sample by a water path, and the sample is further separated from the reflector plate by another water path. The pulse-echo distances (twice the distance traveled by the ultrasonic beam to the reflector plate) for various set-ups can become significant at times. Because of this, it may be important to consider the effects of diffraction (beam spread) on absolute velocity values if using unfocused transducers such as was done in the silicon nitride scans. Beam spreading becomes an issue at distances from the transducer greater than that defined by the near field or Fresnel length (Z') (Ref. A1). The net effect of beam spreading is to make an echo smaller and shifted in time, with the effect becoming more significant as distance from transducer is increased. Near field length (Z') is defined by:

$$Z' = \frac{a^2}{\lambda} = a^2\left(\frac{f}{V}\right) \tag{A1}$$

where a is transducer element radius, λ is the ultrasonic wavelength, V is the velocity of ultrasound in the medium, and f is the frequency. A normalized distance (S) can be defined (Ref. A1):

$$S = \frac{Z}{Z'} = \left(\frac{Z}{a^2}\right)\left(\frac{V}{f}\right) \tag{A2}$$

where Z is the path length the ultrasonic beam travels in the pulse-echo configuration. Normalized distance denotes the ratio of actual ultrasonic path length to near field length. Beam spreading becomes significant at normalized distances from the transducer greater than 1. Based on Eq. (A2), Fig. A1 shows the effect of path length, frequency, and transducer radii on normalized distance (S) for a path composed solely of water with $V = 1.48$ mm/μsec.

For our simulation, the experimental set-up utilized to obtain the TIRP image of the ceramic disk of Fig. 6(a) in the body of the article was modeled. Curves of diffraction loss and phase shift as a function of normalized distance were obtained from Ref. A1 and used to correct for diffraction effects the ultrasonic echoes obtained for the ceramic disk. The TIRP velocity image was subsequently recalculated by cross-correlating the corrected echoes. Diffraction effects are dependent on ultrasonic bandwidth and a choice of curves from Ref. A1 are available based on transducer bandwidth. Since a broadband transducer of 20 MHz nominal center frequency was employed in the silicon nitride scans, curves for 120 percent (widest) bandwidth were used (Ref. A1) These curves are shown in Fig. A2 with Fig. A2(a) showing loss in nepers (having been converted from dB given in Ref. A1).

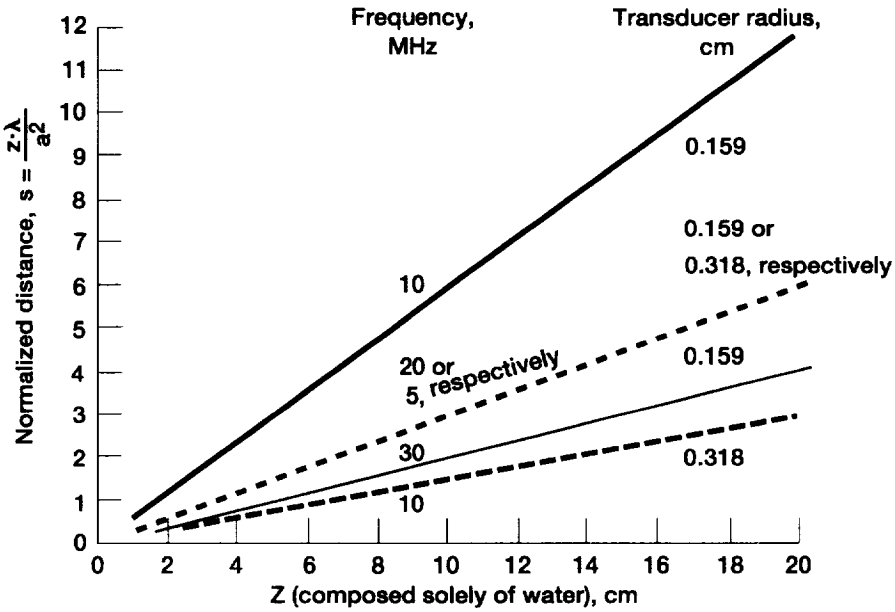

A1.—Normalized distance versus water path length for various transducer frequencies and radii. z = path length of ultrasonic beam, λ = ultrasonic wavelength, a = transducer radius.

Since each echo at each scan point was diffraction-corrected, normalized distance (S) was calculated for echoes B1 (first echo off sample back surface), B2 (second echo off sample back surface), M' (first echo off reflector plate with the sample present) and M" (first echo off the reflector plate with the sample removed), respectively (Fig.2 in the body of the article). For the sample echoes,

$$S_{B1} = 2\frac{Lc}{a^2 f} + 2\frac{dV_{SN}}{a^2 f} \tag{A3a}$$

where S_{B1} is the normalized distance for echo $B1$, L and d are the length of the water path and thickness of the sample, respectively, and c and V_{SN} are the velocity in water and silicon nitride sample, respectively. Similarly:

$$S_{B2} = 2\frac{Lc}{a^2 f} + 4\frac{dV_{SN}}{a^2 f} \tag{A3b}$$

where S_{B2} is the normalized distance for echo $B2$. For the reflector plate echoes:

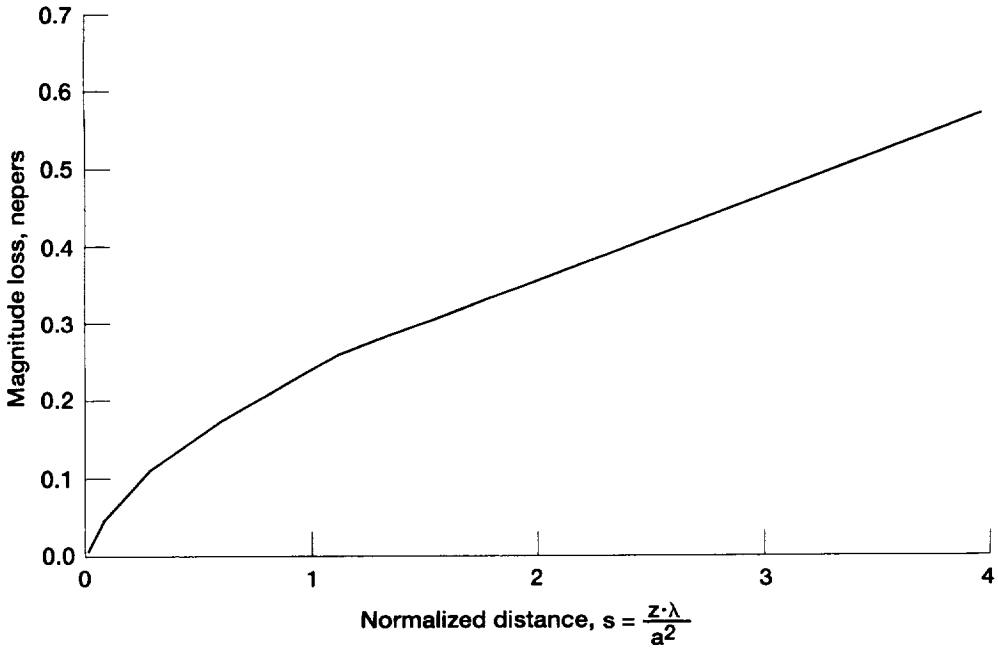

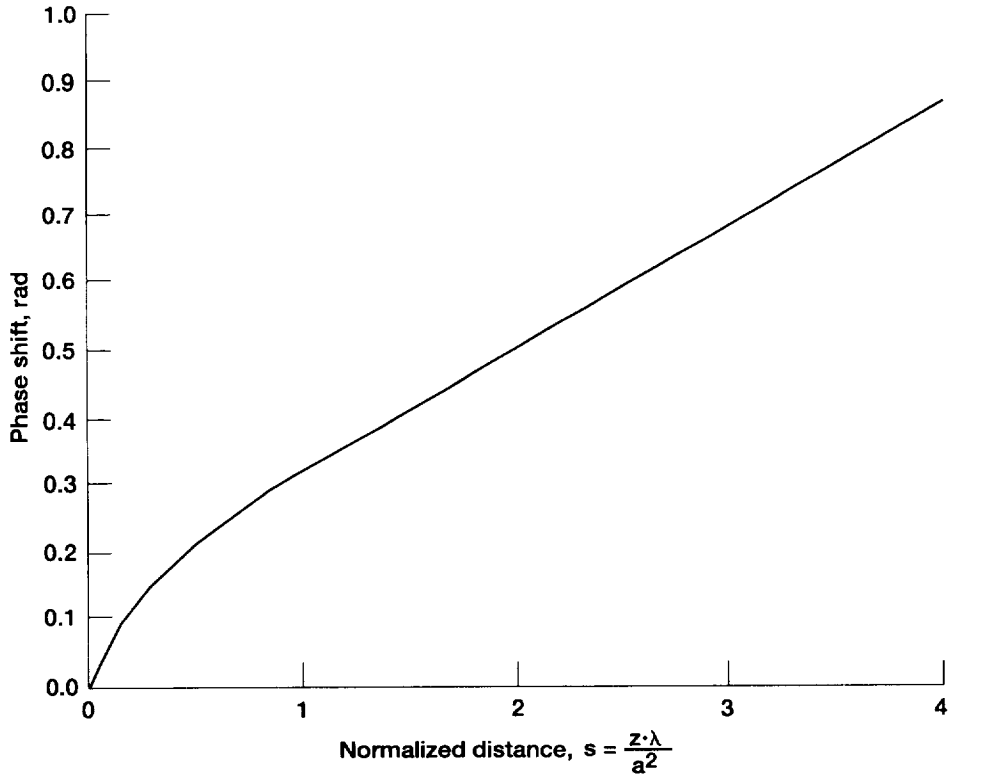

A2.—Magnitude loss and phase shift versus normalized distance (120% bandwidth) resulting from beam spreading (diffraction) from ref. A1. (a) Magnitude loss versus normalized distance. (b) Phase shift versus normalized distance. z =path length of ultrasonic beam λ = ultrasonic wavelength, a = transducer radius.

$$S_{M'} = 2\frac{Lc}{a^2 f} + 2\frac{dV_{SN}}{a^2 f} + 2\frac{L'c}{a^2 f} \tag{A3c}$$

where $S_{M'}$ is the normalized distance for echo M' and L' is the water path length from the sample back surface to the reflector plate front surface. Similarly:

$$S_{M''} = 2\frac{Lc}{a^2 f} + 2\frac{dc}{a^2 f} + 2\frac{L'c}{a^2 f} \tag{A3d}$$

where $S_{M''}$ is the normalized distance for echo M''. In the silicon nitride scans of this study, c = 1.48 mm/μsec, V_{SN} = the velocity obtained at that particular scan point, L = 4 cm, L' = 1.3 cm, a = 0.159 cm and f = a frequency contained within each broadband echo.

To apply diffraction corrections and then recalculate the velocity image, a fortran program was written inwhich:

(1) the curves of Fig. A2(a) and (b) were divided into discrete values allowing the computerized application of diffraction corrections as a function of normalized distance (S) for each echo.

(2) For each of time-domain echoes $B1$, $B2$, M', and M'' at each scan point:

(a) the echo was fast-fourier-transformed into the frequency domain to obtain real and imaginary coefficients which were subsequently used to obtain magnitude and phase spectra. 2π radians were subtracted from phase spectra at discrete frequencies where needed to make phase spectra continuous (phase unwrapping procedure) as a function of frequency (Ref. A2).

(b) Normalized distance (S) was determined at each frequency of the spectra of the fourier-transformed echoes according to Eqs. A3(a) to (d).

(c) the magnitude at each frequency within the spectra was corrected for loss according to:

$$CMAG(f) = MAG(f) x 10^{(\text{loss}/20)} \tag{A4}$$

where $CMAG(f)$ and $MAG(f)$ are the diffraction-corrected and original magnitudes at a particular frequency, respectively, and loss is in nepers. The value of loss was determined as a function of normalized distance from Fig. A2(a) according to step 1.

(d) the phase at each frequency within the spectra was corrected for phase shift according to:

$$CPHA(f) = PHA(f) + shift \tag{A5}$$

where $CPHA(f)$ and $PHA(f)$ are the diffraction-corrected and original phase at a particular frequency, respectively, and shift is the phase shift in radians. The value of phase shift was determined as a function of normalized distance from Fig. A2(b) according to step 1.

(e) Two reconstructions were performed for each fourier-transformed echo. Fourier-transformed echoes having corrected magnitude only, and corrected magnitude and phase were reconstructed in the time domain by performing inverse-fast-fourier-transformation. The former was performed to test for consistent echo polarity. It was found that in some cases, magnitude-only corrected echoes were ~π radians out-of-phase (or inverted) compared to original time-domain echoes. This is an incorrect result since no phase corrections were applied and is thought to be due to a signal processing anomaly. Phase inversion such as this results in improper cross-correlations and thus improper velocities. For such cases, the same echoes having been corrected for both magnitude and phase were inverted so that correct polarity was restored.

(f) A cross-correlation algorithm (Ref. A3) was performed to obtain time delays between reconstructed $B1$ and $B2$ echoes, and between reconstructed M' and M'' echoes. Phase relationships were examined for $B1$ compared to $B2$ and M' compared to M'' before implementing the algorithm. If the echoes were not phase-inverted with respect to each other, the time occurrence of the *maximum* in the correlation function was used to calculate time delay. If the echoes were phase-inverted, the time occurrence of the *minimum* in the correlation function was used to calculate time delay.

(g) velocity was recalculated according to Eq. (9) in the body of the article.

Figure A3 shows a set of original and diffraction-corrected magnitude and phase spectra, and time-domain waveforms, for a scan point in the center of the silicon nitride disk. Figure A4 shows the TIRP velocity images of the disk before and after diffraction corrections. It can be seen that for the experimental set-up of this investigation, diffraction effects were negligible. Diffraction-corrected velocity values were on the order of 0.5 percent greater than original velocity values.

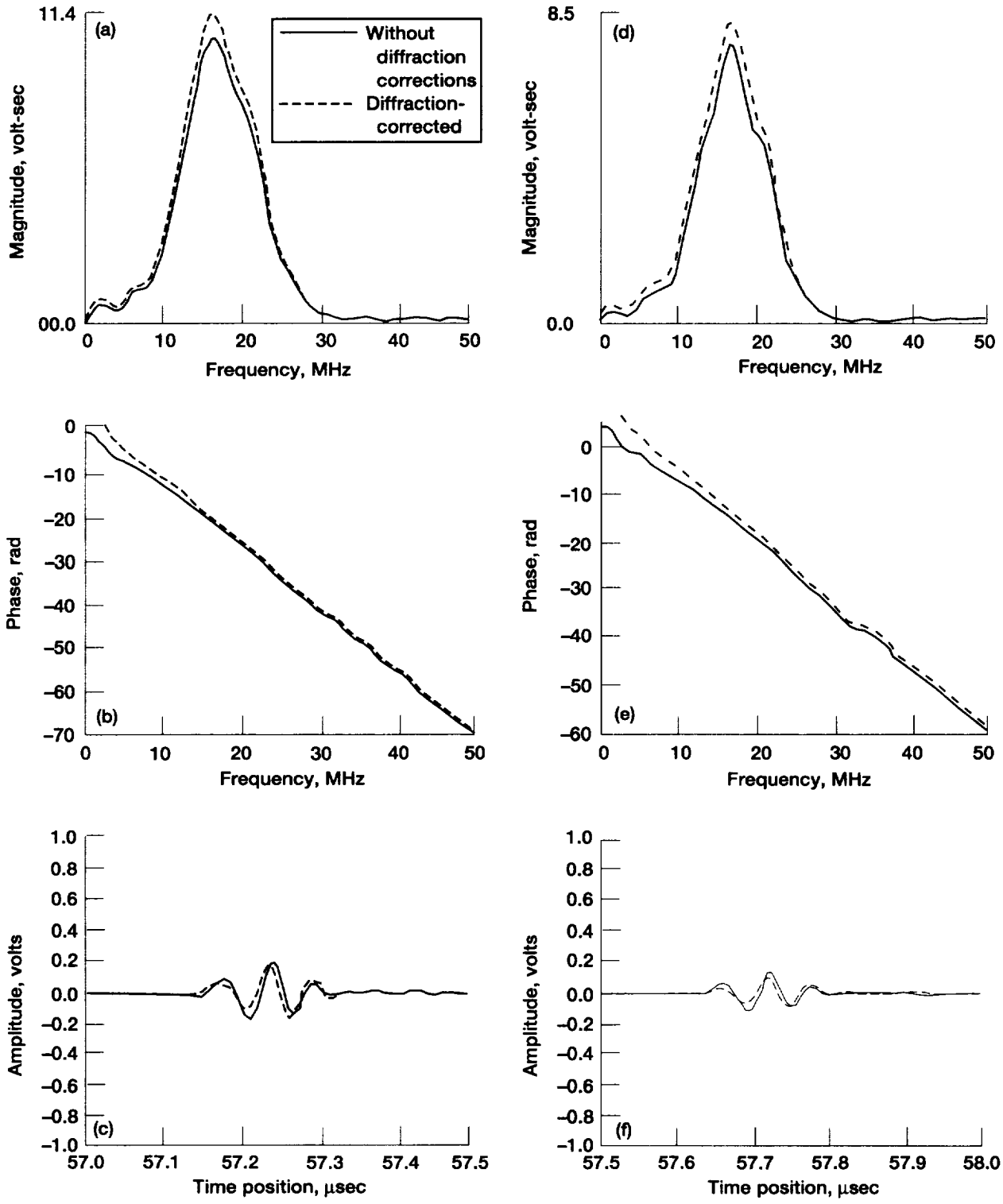

A3.—Set of non-diffraction-corrected and diffraction-corrected magnitude, phase spectra, and time-domain waveforms for scan point at center of silicon nitride disk. (a) B1 Magnitude spectra. (b) B1 Phase spectra. (c) B1 Time domain wave. (d) B2 Magnitude spectra. (e) B2 Phase spectra. (f) B2 Time domain wave. (g) M' Magnitude spectra. (h) M' Phase spectra. (i) M' Time domain wave. (j) M"magnitude spectra. (k) M" Phase spectra. (l) M" Time domain wave.

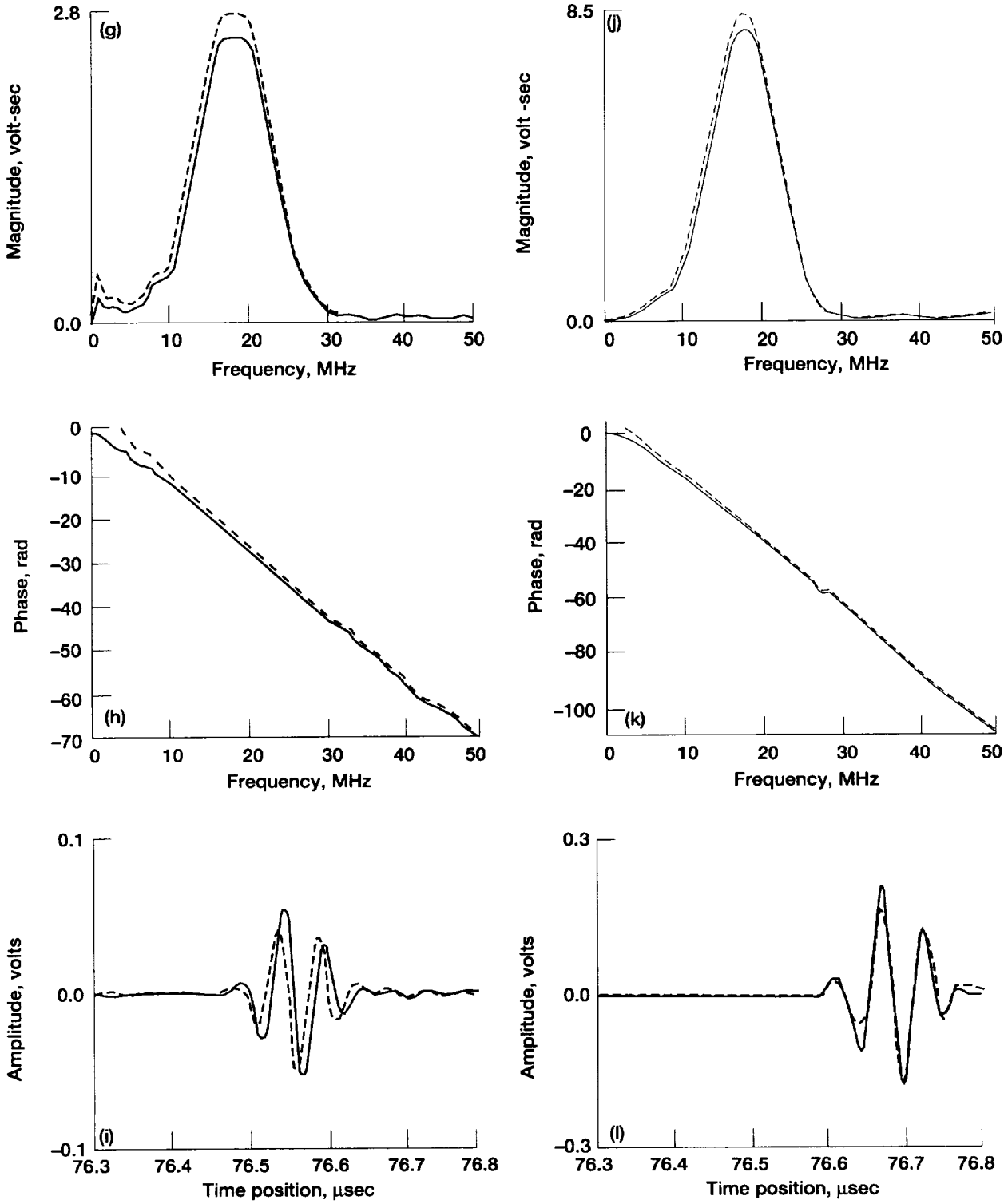

A3.—Concluded. (g) M' Magnitude spectra. (h) M' Phase spectra. (i) M' Time domain wave. (j) M" magnitude spectra. (k) M" Phase spectra. (l) M" Time domain wave.

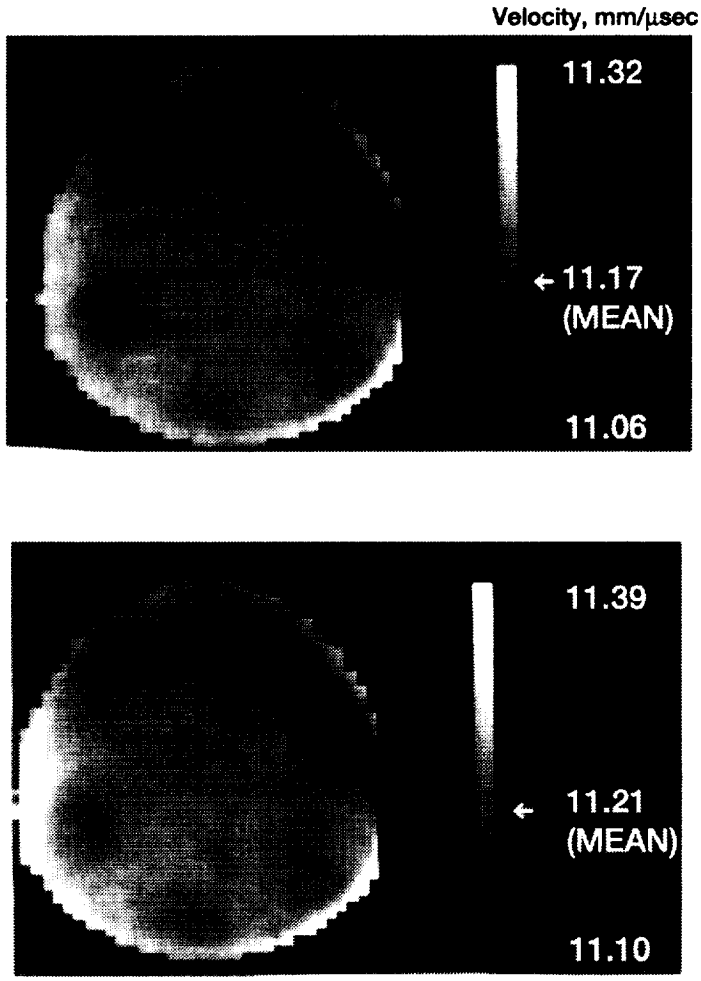

A4.—Thickness-independent velocity images of silicon nitride disk before and after diffraction corrections. (a) Before diffraction corrections. (b) After diffraction corrections.

APPENDIX REFERENCES

A1. Papadakis, E.P.: Ultrasonic Diffraction from Single Apertures with Application to Pulse Measurements and Crystal Physics, Physical Acoustics, Vol. XI, 1975. edited by W.P. Mason and R.N. Thurston, Academic Press. pp. 173–178.

A2. Sachse, W. and Pao, Y.H.: On the Determination of Phase and Group Velocities of Dispersive Waves in Solids. J. Appl. Phys., Vol. 39, 1978, p. 4320.

A3. Hull, D.R.; Kautz, H.E.; and Vary, A.: Measurement of Ultrasonic Velocity Using Phase-Slope and Cross-Correlation Methods. Mater. Eval., vol. 43, no. 11, 1985, pp. 1455–1460.

A4. Nondestructive Testing Handbook, second edition, Volume 7 Ultrasonic Testing, eds. Birks, A.S., Green, R.E., and McIntire, P. American Society For Nondestructive Testing, 1991, pp. 225.

REPORT DOCUMENTATION PAGE

Form Approved
OMB No. 0704-0188

1. AGENCY USE ONLY (*Leave blank*)	2. REPORT DATE	3. REPORT TYPE AND DATES COVERED
	July 1996	Technical Memorandum

4. TITLE AND SUBTITLE

Single Transducer Ultrasonic Imaging Method that Eliminates the Effect of Plate Thickness Variation in the Image

5. FUNDING NUMBERS

WU-505-63-12

6. AUTHOR(S)

Don J. Roth

7. PERFORMING ORGANIZATION NAME(S) AND ADDRESS(ES)

National Aeronautics and Space Administration
Lewis Research Center
Cleveland, Ohio 44135-3191

8. PERFORMING ORGANIZATION REPORT NUMBER

E-10151

9. SPONSORING/MONITORING AGENCY NAME(S) AND ADDRESS(ES)

National Aeronautics and Space Administration
Washington, D.C. 20546-0001

10. SPONSORING/MONITORING AGENCY REPORT NUMBER

NASA TM-107184

11. SUPPLEMENTARY NOTES

Responsible person, Don J. Roth, organization code 5250, (216) 433-6017.

12a. DISTRIBUTION/AVAILABILITY STATEMENT

Unclassified - Unlimited
Subject Category 38

This publication is available from the NASA Center for AeroSpace Information, (301) 621-0390.

12b. DISTRIBUTION CODE

13. ABSTRACT (*Maximum 200 words*)

This article describes a single transducer ultrasonic imaging method that eliminates the effect of plate thickness variation in the image. The method thus isolates ultrasonic variations due to material microstructure. The use of this method can result in significant cost savings because the ultrasonic image can be interpreted correctly without the need for machining to achieve precise thickness uniformity during nondestructive evaluations of material development. The method is based on measurement of ultrasonic velocity. Images obtained using the thickness-independent methodology are compared with conventional velocity and c-scan echo peak amplitude images for monolithic ceramic (silicon nitride), metal matrix composite and polymer matrix composite materials. It was found that the thickness-independent ultrasonic images reveal and quantify correctly areas of global microstructural (pore and fiber volume fraction) variation due to the elimination of thickness effects. The thickness-independent ultrasonic imaging method described in this article is currently being commercialized under a cooperative agreement between NASA Lewis Research Center and Sonix, Inc.

14. SUBJECT TERMS

Ultrasonics; Thickness; Velocity; Technology transfer

15. NUMBER OF PAGES

36

16. PRICE CODE

A03

17. SECURITY CLASSIFICATION OF REPORT	18. SECURITY CLASSIFICATION OF THIS PAGE	19. SECURITY CLASSIFICATION OF ABSTRACT	20. LIMITATION OF ABSTRACT
Unclassified	Unclassified	Unclassified	

National Aeronautics and
Space Administration

Lewis Research Center
21000 Brookpark Rd.
Cleveland, OH 44135-3191